# Binding of Protoporphyrin IX and Metal Derivatives to the Active Site of Wild-Type Mouse Ferrochelatase at Low Porphyrin-to-Protein Ratios†

Yi Lu,‡ Adelaide Sousa,§,|| Ricardo Franco,*,‡,|| Arianna Mangravita,§ Gloria C. Ferreira,*,§ Isabel Moura,|| and John A. Shelnutt*,‡

*Biomolecular Materials and Interfaces Department, Sandia National Laboratories, Albuquerque, New Mexico 87185-1349, Department of Chemistry, University of New Mexico, Albuquerque, New Mexico 87131, Department of Biochemistry and Molecular Biology, College of Medicine, Institute for Biomolecular Science, and H. Lee Moffitt Cancer Center and Research Institute, University of South Florida, Tampa, Florida 33612, and Centro de Química Fina e Biotecnologia, Departamento de Química, Faculdade de Ciências e Tecnologia, Universidade Nova de Lisboa, 2829−516 Caparica, Portugal*

*Received January 22, 2002; Revised Manuscript Received May 8, 2002*

ABSTRACT: Resonance Raman (RR) spectroscopy is used to examine porphyrin substrate, product, and inhibitor interactions with the active site of murine ferrochelatase (EC 4.99.1.1), the terminal enzyme in the biosynthesis of heme. The enzyme catalyzes in vivo $Fe^{2+}$ chelation into protoporphyrin IX to give heme. The RR spectra of native ferrochelatase show that the protein, as isolated, contains varying amounts of endogenously bound high- or low-spin ferric heme, always at much less than 1 equiv. RR data on the binding of free-base protoporphyrin IX and its metalated complexes (Fe(III), Fe(II), and Ni(II)) to active wild-type protein were obtained at varying ratios of porphyrin to protein. The binding of ferric heme, a known inhibitor of the enzyme, leads to the formation of a low-spin six-coordinate adduct. Ferrous heme, the enzyme's natural product, binds in the ferrous high-spin five-coordinate state. Ni(II) protoporphyrin, a metalloporphyrin that has a low tendency toward axial ligation, becomes distorted when bound to ferrochelatase. Similarly for free-base protoporphyrin, the natural substrate of ferrochelatase, the RR spectra of porphyrin−protein complexes reveal a saddling distortion of the porphyrin. These results corroborate and extend our previous findings that porphyrin distortion, a crucial step of the catalytic mechanism, occurs even in the absence of bound metal substrate. Moreover, RR data reveal the presence of an amino acid residue in the active site of ferrochelatase which is capable of specific axial ligation to metals.

The last step of the heme biosynthetic pathway, the insertion of ferrous iron into protoporphyrin IX[1] to give heme, is catalyzed by ferrochelatase (protoheme ferrolyase, EC 4.99.1.1) (*1*). Ferrochelatases can be broadly classified into two categories, namely, the [2Fe-2S]-cluster-containing ferrochelatases, a class that includes murine (*2*) and human (*3*) ferrochelatases, and the ferrochelatases that lack the iron−sulfur cofactor. The enzymes from *Bacillus subtilis* and *Saccharomyces cerevisiae* belong to the latter class. The three-dimensional 1.9-Å X-ray crystal structure of *B. subtilis* ferrochelatase revealed a monomeric state for the protein and an active site cleft where several amino acid residues that are conserved among all known ferrochelatase sequences are located (*4*). The equivalent conserved residues were also identified at the active site of human ferrochelatase, as disclosed by the 2.0-Å X-ray crystal structure of this enzyme (*5*). Human ferrochelatase is a homodimer, with the active sites oriented parallel to each other at a protruding hydrophobic surface that presumably functions as a mitochondrial membrane anchor. The iron−sulfur cluster, located distantly from the active site, might have an indirect role in protein dimerization.

The catalytic mechanism of ferrochelatase has been proposed to involve an out-of-plane distortion of the porphyrin substrate; the distortion facilitates the reaction by exposing the pyrrole nitrogens to the incoming metal ion (*6*). Such a nonplanar distortion is present in *N*-alkyl porphyrins, which are strong inhibitors of the enzyme (*7*, *8*). This observation leads to the suggestion that *N*-methylporphyrins are transition-state analogues. This idea received further support from an antibody raised against *N*-methyl mesoporphyrin that catalyzed metal insertion into the porphyrin ring (*9*, *10*).

Cocrystallization of *B. subtilis* ferrochelatase with the potent inhibitor *N*-methyl mesoporphyrin revealed that only

† Sandia is a multiprogram laboratory operated by Sandia Corporation, a Lockheed Martin Company, for the United States Department of Energy under Contract DE-AC04-94AL85000. This work was supported by FLAD (Luso American Development Foundation) (to G.C.F., I.M., and R.F.), the American Cancer Society (Grant RPG-96-051-04-TBE), the American Heart Association, Florida Affiliate (Grant 0051240B) (to G.C.F.), and Fundação para a Ciência e Tecnologia (POCTI/34973/BME/2000 to R.F. and PRAXIS XXI/BD16084/98 scholarship to A.S.)

* To whom correspondence should be addressed. (Professor John A. Shelnutt) Phone: 505-272-7160. Fax: 505-272-7077. E-mail: jasheln@unm.edu. (Professor Gloria C. Ferreira) Phone: 813-974-5797. Fax: 813-974-0504. E-mail: gferreir@hsc.usf.edu.

‡ Sandia National Laboratories and University of New Mexico.

§ University of South Florida.

|| Universidade Nova de Lisboa.

[1] Abbreviations: ProtoP, protoporphyrin IX; OEP, octaethylporphyrin; Ni-Hb, nickel-reconstituted hemoglobin A; CTAB, cetyltrimethylammonium bromide; SDS, sodium *n*-dodecyl sulfate; CMC, critical micellar concentration; $K_D$, equilibrium dissociation constant; UV, ultraviolet; RR, resonance Raman; CCD, charge-coupled device.

10.1021/bi025569m CCC: $22.00 
Published on Web 06/08/2002

one of its eight isomers binds to the active site of the protein (*11*). The selected isomer, when bound to the protein, shows a tilt angle of about 36° with respect to the mean porphyrin plane for pyrrole ring A. Most of this distortion undoubtedly results from steric repulsion between the *N*-methyl substituent and the central core of the porphyrin ring. However, it was reported (*11*) that a similar tilt of ring A also occurs for copper protoporphyrin bound at the active site of the enzyme, the distortion seemingly imposed by the interaction of the copper protoporphyrin with a tyrosine residue. Overall, these porphyrins exhibit a macrocyclic distortion composed primarily of a mixture of ruffle- and saddle-type deformations (*12*−*14*). These crystallographic results thus suggest that this type of distorted structure is adopted by the protein-bound free-base porphyrin substrate. The crystallographic results are also in good agreement with the conclusion that *N*-methylporphyrins are transition-state analogues for porphyrin metalation (*9*). RR studies on murine ferrochelatase show that the porphyrin substrate is in fact somewhat distorted when bound to the protein, even in the absence of the substrate metal ion (*15*). In contrast, RR studies of yeast (*S. cerevisiae*) ferrochelatase incubated with mesoporphyrin IX demonstrated that appreciable porphyrin distortion occurs only upon addition of mercury(II) (*16*). On the other hand, this particular metal ion was found to irreversibly denature mouse ferrochelatase (*15*).

In the present study, the resonance Raman spectral changes associated with binding of several porphyrins to ferrochelatase are examined under conditions which amplify the RR spectra of the porphyrin bound specifically to the protein. Besides studies of the $H_2$(ProtoP)−ferrochelatase substrate complexes, RR examination of Ni(ProtoP)−ferrochelatase complex provides valuable information about the distortion forces exerted by the protein on the porphyrin macrocycle because this metalated porphyrin is particularly sensitive to out-of-plane deformations. We had already observed shifts in the structure-sensitive lines of Ni(ProtoP) upon binding to ferrochelatase when compared to the spectra obtained for the porphyrin in detergent solutions (*15*). In this study, the binding of ferric heme, a known inhibitor of ferrochelatase activity (*8*), is also investigated, and the ferric heme is found to bind to the protein as a hexa-coordinated complex. Finally, ferrous heme, the natural product of ferrochelatase, binds in a five-coordinate high-spin fashion. This latter result was confirmed by a UV−visible titration of the enzyme with ferrous heme.

Removal of interference from the unbound and weakly bound porphyrin is crucial to obtaining spectra of the specifically bound porphyrin species and determining the protein-induced changes in porphyrin structure. To accomplish this, substoichiometric amounts of nickel protoporphyrin [Ni(ProtoP)], iron protoporphyrin [Fe(ProtoP)], and free-base protoporphyrin [$H_2$(ProtoP)] were complexed with the wild-type enzyme. In this way, information could be obtained from the relative stronger spectrum of the specifically bound porphyrin with less interference from the intense spectra of loosely bound or unbound porphyrin which is also present. In addition, RR data were collected both in the high-frequency (1300−1700 $cm^{-1}$) and in the low-frequency (250−800 $cm^{-1}$) regions. The low-frequency region of the RR spectra, not provided in the previous study (*15*), gives valuable information on several out-of-plane modes, structure-sensitive modes, and substituent modes of porphyrins. Changes in these additional modes are instrumental in defining the protein-induced distortion. These RR spectroscopic studies establish a more complete view of porphyrin binding to murine ferrochelatase.

## MATERIALS AND METHODS

*Materials.* The porphyrins used in these studies were purchased from Porphyrin Products (Logan, UT) except for ferric heme, which was purchased from Sigma-Aldrich (St. Louis, MO). Porphyrins were used without further purification. The bicinchoninic acid protein assay reagents were purchased from Sigma-Aldrich. Acrylamide and gel reagents were purchased from Bio-Rad (Hercules, CA). Ni-NTA agarose was from Qiagen (Basel, Switzerland). All other chemicals were of the highest purity available.

*Enzyme Preparation.* Recombinant murine liver ferrochelatase was isolated from hyperproducing DH5α *Escherichia coli* cells containing the ferrochelatase expression plasmid pGF47 and purified and assayed for activity, as previously described (*17*). Aliquots of 200 μL of typically 150 μM concentrated protein in buffer H (20 mM Tris-HCl (pH 8), 10% glycerol, and 0.5 M NaCl) were frozen and stored in liquid nitrogen until use. The protein was reduced with a 30 mg/mL sodium hydrosulfite solution made in Tris-HCl buffer (0.1 M, pH 9).

*Porphyrin Solutions.* Porphyrin stock solutions were prepared by dissolving the powder reagent in 100 μL of 2 M $NH_4OH$ with vigorous shaking and then adding 100 μL of 20% (w/v) Tween 80 and 2 mL of water. Further dilutions of porphyrin solutions were made in 0.1 M Tris-HCl buffer at pH 8. Ferrous heme samples were prepared by reducing a ferric heme solution with a 30 mg/mL sodium hydrosulfite solution in Tris-HCl buffer (0.1 M, pH 9). The ferric heme $CN^-$ complex was prepared by adding potassium cyanide salt to a ferric heme solution buffered at pH 8 with Tris-HCl at 0.1 M.

*Spectroscopy.* Raman samples were prepared in buffer H with Tween 80 added so that the final concentration of detergent in the Raman cell was 55 μM. This Tween 80 concentration was chosen for comparison with previously published work (*18*, *19*), which utilized similar detergent concentration, and because this detergent concentration gave good fluorescence and absorption spectra of the porphyrin as well as good kinetic traces. In addition, kinetic studies show an increase in ferrochelatase activity up to 50 μM Tween. Above this detergent concentration, the activity stays at about the same value until much higher detergent concentration causes the activity to decrease significantly. The detergent concentration of 55 μM in Tween 80 is 4.5 times the CMC value, ensuring that micellar structures are present. However, under these conditions for which there are many more porphyrin molecules than detergent micelles present, the detergent molecules must be viewed as intercalating into porphyrin aggregates rather than the porphyrin molecules residing within detergent micelles, as would be the case for high detergent-to-porphyrin molar ratios (*20*). Nevertheless, the porphyrins have a monomer-like absorption spectrum (narrow and redshifted). In addition, RR spectra of the porphyrins in detergent solutions of a variety of detergents (CTAB, SDS, sodium cholate, and deoxycholic

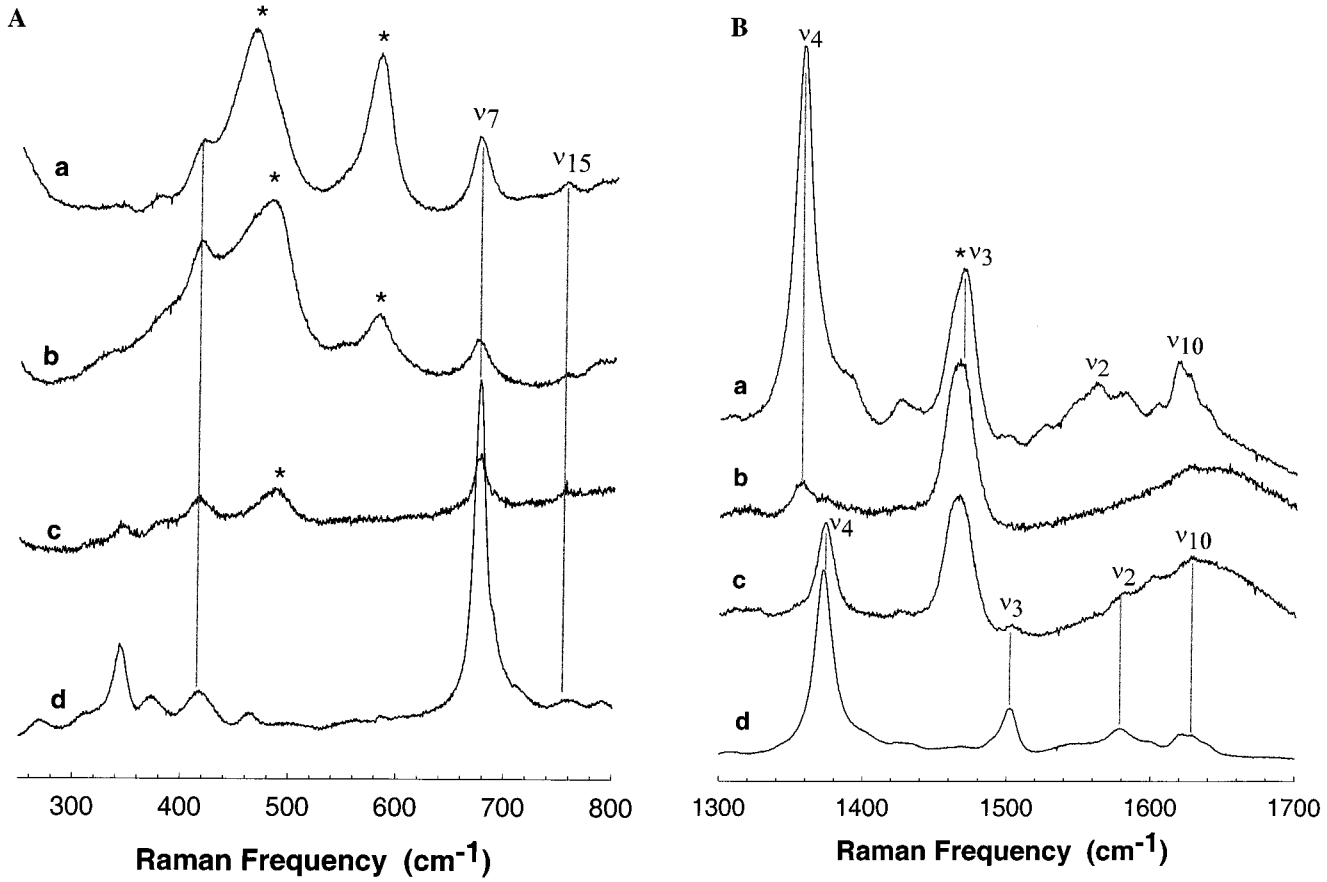


FIGURE 1: Low-frequency (A) and high-frequency (B) regions of the resonance Raman spectra of (a) sodium hydrosulfite-reduced ferrous heme, (b) reduced wild-type ferrochelatase, (c) native wild-type ferrochelatase, and (d) low-spin ferric heme ($CN^-$ complex) in buffer H with Tween 80. The asterisks denote buffer or dithionite lines.

acid (data not shown)) with different charges, different micellar shapes, and at different concentrations above the CMC gave almost identical RR spectra (except for Ni(ProtoP)). The low detergent concentration also minimizes the interference from the detergent Raman spectrum and fluorescence.

The appropriate volumes of the respective stocks of porphyrin and ferrochelatase, buffer H, and detergent solution in water were added for a final volume of 50−100 $\mu$L in a stoppered 3 × 3 mm cross-sectional optical cell (NSG Precision Cells, Farmingdale, NY). The Raman samples were kept in ice until immediately before the spectra were obtained, typically at room temperature (26 °C) in 2−10 min using 20 mW of laser power in a partially focused beam.

RR spectra were obtained using the 406.7-nm line of an INNOVA 302 $Kr^+$ laser (Coherent) and using a Raman spectrometer described previously (*15*). Briefly, the spectrometer is a 0.75-m monochromator with a 2048-channel CCD detector (Instruments, SA). The slit width of 100 $\mu$m gives a spectral resolution of 2 $cm^{-1}$. Position mode was used for CCD detection, with each section covering about 500 $cm^{-1}$ of the Raman spectrum without moving the grating. Spectra were output from the computer controller for plotting with SigmaPlot (SPSS).

The UV−visible absorption spectra were recorded on a HP9852A diode array spectrophotometer in 1-cm quartz optical cells. The same buffer system was used as for the RR samples.

## RESULTS

*Endogenously Bound Ferric Heme in the Native Protein.* As isolated, native wild-type ferrochelatase contains minor and variable amounts of ferric porphyrin endogenously bound to the protein. That is, ferric heme stays bound to the protein during the purification procedure. This conclusion is based on the RR spectra of ferrochelatase obtained in this study and the spectra of native ferrochelatase observed in previous work (*15*). In the RR spectra of the isolated protein in the previous study, a few unidentified weak Raman lines were observed, and these lines have now been identified as those of ferric heme by comparison with the RR spectra of various metal porphyrins under similar solvent conditions. The RR spectra for native and hydrosulfite-reduced ferrochelatase, together with high-spin ferrous and low-spin ferric heme ($CN^-$ complex) models, are presented in Figure 1A,B for the low-frequency and high-frequency regions, respectively, and the frequencies of the lines are listed in Table 1. The RR spectrum of native enzyme has the major characteristic features of endogenously bound low-spin ferric heme with the oxidation-state marker line $\nu_4$ at 1373 $cm^{-1}$, $\nu_3$ at 1503 $cm^{-1}$, and $\nu_{10}$ at 1628 $cm^{-1}$ (Figure 1B, spectrum c). The frequencies of the latter two structure-sensitive lines, especially $\nu_3$, are indicative of the low-spin state, and the spectra compare favorably with the spectrum of the model $CN^-$ complex (Figure 1B, spectrum d). Thus, the endogenously bound porphyrin is consistent with low-spin six-coordinate ferric heme for the preparation used in the present study

Table 1: Frequencies ($cm^{-1}$) of Some of the Structure-Sensitive Raman Lines of Native Wild-Type Ferrochelatase in Both the High-Frequency (1300−1700 $cm^{-1}$) and the Low-Frequency (250−800 $cm^{-1}$) Regions with and without Bound Ferric Heme, Ni(ProtoP), and $H_2$(ProtoP) and for These Porphyrins in Other Environments[a]

| | $\nu_{10}$ | $\nu_{Ca=Cb}$ | $\nu_2$ | $\nu_3$ | $\nu_4$ | $\nu_{15}$ | $\nu_7$ | $\delta_{C\beta CaCb}$ | $\nu_{Prop}$ | $\nu_8$ |
|---|---|---|---|---|---|---|---|---|---|---|
| | | | | | Native FC | | | | | |
| buffer | 1628.1 | | 1580.1 | 1503.2 | 1373.1 | 754.9 | 675.7 | 416.5 | | 345.4 |
| | | | | | Reduced FC | | | | | |
| buffer | | | | | 1357.7 | | 673.9 | 416.5 | | |
| | | | | | Ferrous Heme | | | | | |
| FC, 0.5 | 1617.8 | | 1561.9 | 1468.6 | 1356.9 | | 673 | 416.8 | 376.9 | |
| | | | | | Ferric Heme | | | | | |
| buffer | 1625.3 | | 1568.3 | 1489.3 | 1372 | 754.7 | 674.9 | 416.8 | 379.7 | 348.5 |
| $CN^-$ complex | | | 1578.6 | 1501.9 | 1372.4 | | 675.9 | 416.7 | 373.8 | 344.5 |
| FC | 1638.2 | | 1578.2 | 1502.8 | 1373 | | 675.8 | 411.6 | 376.4 | 343.7 |
| | | | | | Ni(ProtoP) | | | | | |
| buffer | 1657.8 | 1632 | 1593.2 | 1519.9 | 1379.5 | 752.6 | 684.5 | 418.7 | 379.9 | 344.5 |
| | | | | | | | 676.2 | | 369.6 | |
| FC | 1655.2 | 1632.8 | 1589.2 | 1518.7 | 1378.8 | 752.8 | 687.4 | 417.6 | 386.6 | 342.9 |
| | | | | | | | 672.6 | | 372.1 | |
| | | | | | $H_2$(ProtoP) | | | | | |
| buffer | 1612.8 | | 1538.7 | 1479.7 | 1367.9 | | 663.4 | | | |
| FC | 1626.1 | | | 1489.4 | 1369.4 | | 673.9 | 415.6 | 378.7 | 345.4 |

[a] Data for bound porphyrins are for samples with a 10-fold excess of protein in relation to porphyrin.

(Figure 1, spectrum c). This was confirmed by reduction of the endogenously bound ferric heme with sodium hydrosulfite (Figure 1, spectrum b). Upon reduction, $\nu_4$ downshifts 15.4 $cm^{-1}$ (see Table 1), indicating the conversion of ferric into ferrous iron; $\nu_4$ is in good agreement with the high-spin ferrous heme model under the same solvent conditions (Figure 1, spectrum a). Hydrosulfite reduction also verified that previous ferrochelatase preparations, which also had the same catalytic activity as that utilized in the present work, contained endogenously bound high-spin ferric heme. The cause of the variability in the spin state of the endogenously bound ferric heme in different preparations of the protein has not been determined, but the activity of the enzyme is unaffected. This variability will be discussed further in the following sections.

*Binding of Ferrous Heme to Ferrochelatase.* Titration of ferrochelatase with Fe(II)(ProtoP), as observed by UV−visible absorption spectroscopy, can reveal the binding of the heme to the enzyme as well as the spin state of the heme iron (data not shown). Upon adding substoichiometric amounts of ferrous heme (ratio = 0.1) to a protein solution under anaerobic conditions, the Soret peak for heme narrowed and redshifted from below 400 nm for free ferrous heme in buffer to 426 nm when reacted with the protein, indicating binding to ferrochelatase. At higher concentrations of porphyrin (ratio = 1.0, 3.0), the Soret band shifts back to the blue ($\lambda_{max}$ = 424, 422 nm) as the concentration of unbound ferrous heme increases. The absorption spectra are typical of five-coordinate high-spin ferrous heme. No absorbance peaks near 524 and 556 nm that are characteristic of a low-spin ferrous heme species (such as the Fe(II)(ProtoP) bispyridine adduct (*21*)) were observed.

RR spectra of ferrochelatase with 0.5 equiv of ferrous heme added to the protein solution confirmed these results by revealing the presence of Fe(II)(ProtoP) in a high-spin five-coordinate environment as indicated by frequencies for the spin-state and oxidation-state marker lines that are similar to ferrous heme in the buffered solution (spectrum not shown, see Table 1). Although there are no significant differences between the RR spectra of ferrous heme in buffer and when bound to the protein at a molar ratio of 0.5, nonetheless, the UV−visible titration demonstrates that interaction of ferrous heme with the protein does occur.

*Binding of Ferric Heme to Ferrochelatase.* To analyze the interaction of ferrochelatase with ferric heme, a known inhibitor of the enzyme, RR spectra were obtained for increasing amounts of ferric heme added to protein solutions. Figure 2 depicts the low-frequency (Figure 2A) and high-frequency (Figure 2B) regions of the RR spectra of the protein samples, along with the spectrum of free ferric heme in a mixture of buffer H and the porphyrin buffer for comparison (Figure 2, spectrum a). For ferric heme in buffer, the marker line frequencies (Figure 2B, spectrum a) are all typical of high-spin five-coordinate ferric heme species (Table 1). When ferrochelatase is present (Figure 2, spectra b−e), the protein-bound ferric heme converts to a low-spin six-coordinate form, as indicated by the frequencies of the RR structure-sensitive lines. Furthermore, the spin state and coordination state of the added ferric heme are the same as for the endogenously bound ferric heme. In particular, as the ferric heme-to-protein ratio decreases, the $\nu_3$ line of the unbound heme at 1489 $cm^{-1}$ progressively decreases in intensity, leaving only $\nu_3$ of the bound heme at 1503 $cm^{-1}$, indicating only a low-spin species at the lowest concentration (Figure 2B, spectrum e). The presence of unbound (or weakly bound) ferric heme is most sensitively measured by the intensity of $\nu_3$ at 1489 $cm^{-1}$. Because of the high intensity of $\nu_3$ in this high-spin form relative to other lines and its large frequency difference from the bound form, even the small fraction of unbound heme, which is expected on the basis of the measured $K_D$ (5.3 $\mu$M) and the inhibition constant (2 $\mu$M) (*8*) for ferric heme, is clearly evident in the RR spectra down to a concentration ratio of 0.1.

In the low-frequency region of the RR spectra of the protein with added ferric heme (Figure 2A), there are also shifts in the RR lines when compared to the free ferric heme spectra. Namely, the structure-sensitive line $\nu_8$ appears at 349 $cm^{-1}$ in the spectrum of the free ferric heme but down-

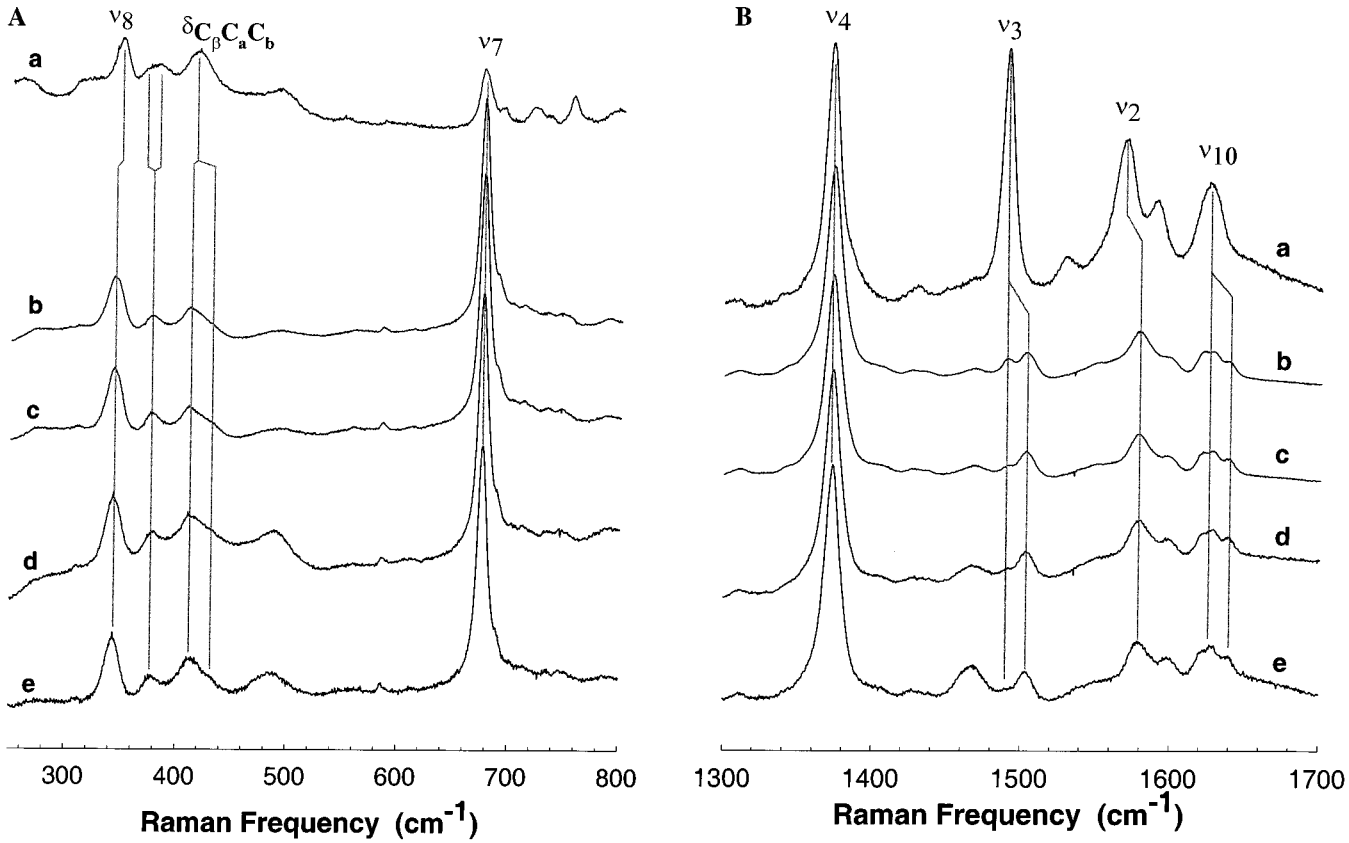


FIGURE 2: Low-frequency (A) and high-frequency (B) regions of the resonance Raman spectra of (a) ferric heme in buffer H with Tween 80 detergent and ferric heme titration of native wild-type ferrochelatase at ferric heme/protein ratios of (b) 1.0 (same concentration of heme as in spectrum a), (c) 0.5, (d) 0.25, and (e) 0.1.

shifts by 4.8 $cm^{-1}$ in the ferrochelatase-bound species. This particular Raman line corresponds to an $A_{1g}$ skeletal mode (*22*) that is known to be sensitive to out-of-plane distortion (*23*). The vinyl bending lines ($\delta_{C\beta CaCb}$) (*22*) near 417 $cm^{-1}$ in the spectrum of the free ferric heme also split, and the lowest frequency component downshifts by 5.2 $cm^{-1}$ when binding to ferrochelatase occurs (Table 1). This spectral change could be associated with changes in the rotational conformation of the vinyl groups that occur upon binding.

*Binding of Ni(ProtoP) to Ferrochelatase.* Our previous studies (*15*) indicated that Ni(ProtoP) binds strongly to ferrochelatase, narrowing and redshifting the Soret band of the porphyrin in the presence of protein. In the present study, we performed a titration of wild-type ferrochelatase with Ni(ProtoP) using RR spectroscopy to gain further insight into the strength and mode of binding to the enzyme of this highly distortion-sensitive metalloporphyrin. Figure 3 depicts the low-frequency (Figure 3A) and high-frequency (Figure 3B) regions of the RR spectra of Ni(ProtoP) itself (Figure 3, spectrum a) and of ferrochelatase with various amounts of added Ni(ProtoP) (Figure 3, spectra b−e). Ni(ProtoP) in a mixture of buffer H and porphyrin buffer (55 $\mu$M in Tween 80) demonstrates a monomer-like RR spectrum. Upon addition of ferrochelatase, the resulting Raman lines of the porphyrin in the high-frequency region of the spectra (Figure 3B, spectra b−e) sharpen, as compared to those of Ni(ProtoP) itself (Figure 3B, spectrum a). In addition, distinct downshifts of the $\nu_3$, $\nu_2$, and $\nu_{10}$ lines are observed upon ferrochelatase binding. The vinyl stretching mode also sharpens and upshifts by 0.8 $cm^{-1}$.

In the low-frequency region of the RR spectra, the changes are even more striking: (1) $\nu_8$ downshifts by 1.6 $cm^{-1}$ and that region of the spectra becomes more complex; (2) the two propionate lines near 375 $cm^{-1}$ change relative intensities; and also (3) the apparent splitting of modes near the $\nu_7$ line for Ni(ProtoP) in detergent micelles increases from 10.3 to 14.4 $cm^{-1}$ when the porphyrin binds to ferrochelatase. By contrast, a single $\nu_7$ line is evident in this region for Ni(ProtoP) in buffer H (data not shown) with a shoulder present on its high-frequency side. Apparently, the splitting derives from the porphyrin being in a special monomer-like state (for a variety of different detergents). Alternatively, the porphyrin is monomeric in the ferrochelatase active site instead of in the $\pi-\pi$ aggregated form, which is the case in buffer without detergent present. However, this $\nu_7$ "splitting" is not observed in the low-frequency RR spectrum of nickel-reconstituted hemoglobin (Ni-Hb) (data not shown), which is known to contain a considerable fraction of monomeric Ni(ProtoP) in a four-coordinate, near-planar state. The latter suggests that the splitting is not simply due to the lack of aggregation of the porphyrin. The splitting of $\nu_7$ is also not observed in other native heme proteins such as cytochrome *c* and myoglobin (*22*, *24*).

The RR spectra of Ni(ProtoP) bound to ferrochelatase at different ratios of Ni(ProtoP) to protein do not exhibit appreciable spectral differences. Spectra at different ratios are all similar with the exception of the 1:1 ratio low-frequency spectrum (Figure 3A, spectrum b), where the RR line of free Ni(ProtoP) at 490 $cm^{-1}$ is more evident. This line probably corresponds to a small contribution from

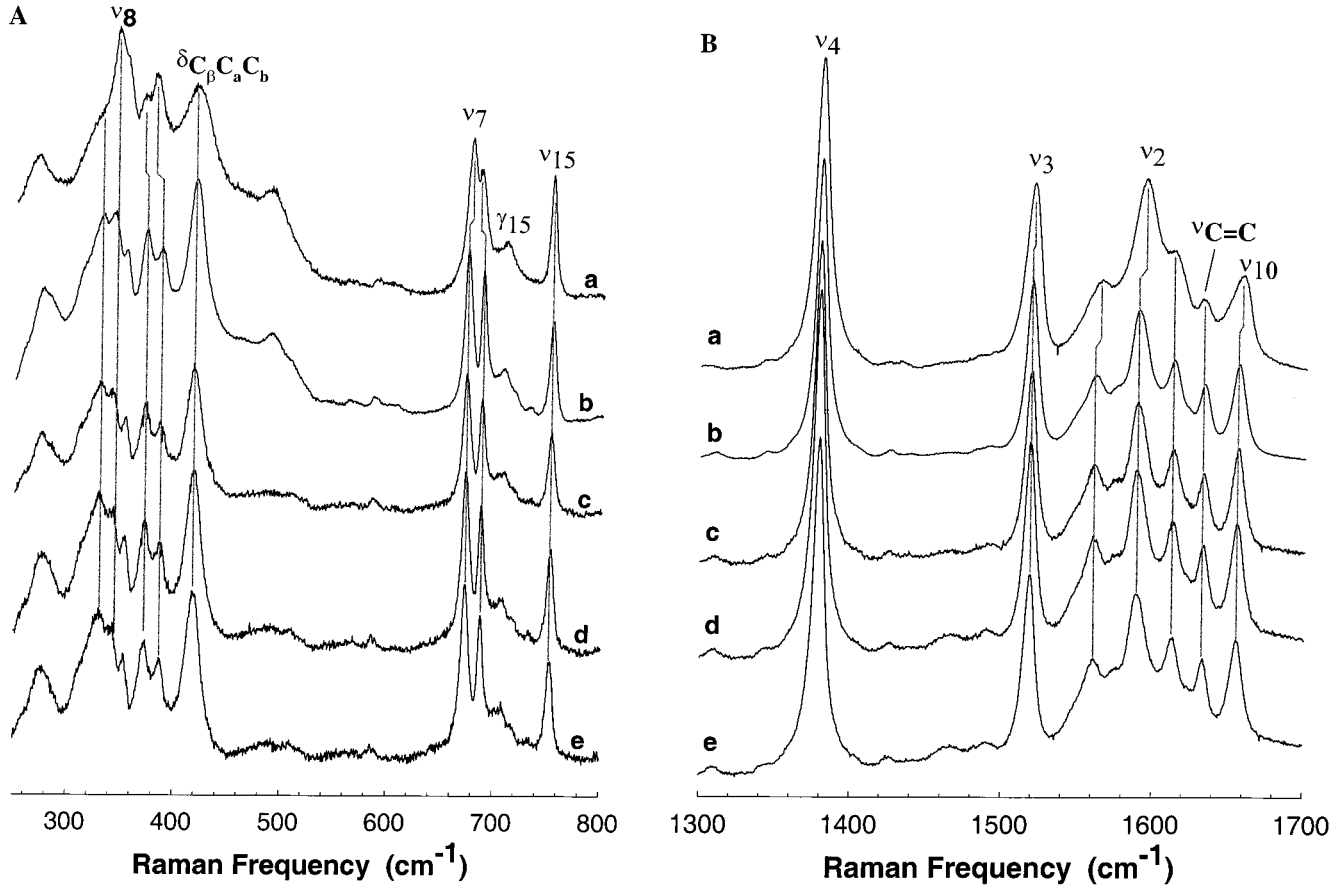


FIGURE 3: Low-frequency (A) and high-frequency (B) regions of the resonance Raman spectra of (a) Ni(ProtoP) in buffer H with detergent, and Ni(ProtoP) titration of native wild-type ferrochelatase at Ni(ProtoP)/protein ratios of (b) 1.0 (same concentration of Ni(ProtoP) as in spectrum a), (c) 0.5, (d) 0.25, and (e) 0.1.

the unbound species since it disappears upon binding at substoichiometric concentrations. This line is probably $\gamma_{22}$, an out-of-plane mode that can also be found in NiOEP (*25*).

*Binding of $H_2$(ProtoP) to Ferrochelatase.* Free-base protoporphyrin IX is the natural substrate of ferrochelatase. Substrate binding at the active site of ferrochelatase was probed for increasing amounts of $H_2$(ProtoP) added to the protein solution using RR spectroscopy. Figure 4 depicts the low-frequency (Figure 4A) and high-frequency (Figure 4B) regions of the RR spectra of ferrochelatase with added $H_2$(ProtoP) at different molar ratios (Figure 4, spectra b−d, f, and g). The RR spectra of $H_2$(ProtoP) in buffer with detergent (Figure 4, spectra a and e) are given for comparison. There are important differences in the RR spectra of the porphyrin bound to ferrochelatase when compared with the micellar environment. In the high-frequency region, $\nu_4$ sharpens and slightly upshifts as the porphyrin-to-protein ratio decreases. The $\nu_3$ line significantly upshifts upon increased protein binding (low molar ratios), going from 1480 $cm^{-1}$ in the detergent solution to 1489 $cm^{-1}$ in the spectrum with the smallest porphyrin-to-protein ratio (0.1) (Figure 4B, spectrum d). The $\nu_2$ line virtually disappears upon protein binding and $\nu_{10}$ upshifts by 13.3 $cm^{-1}$ in the 0.1 porphyrin-to-protein ratio spectrum (Table 1).

Spectra in the low-frequency region (Figure 4A) also exhibit major changes for decreasing porphyrin concentration relative to the protein. The $\nu_7$ line upshifts from 663 $cm^{-1}$ for porphyrin in the detergent solution to 674 $cm^{-1}$ in the protein-bound form. In addition, the $\nu_{16}$ line at 738 $cm^{-1}$ lowers in intensity and in frequency for the bound species. Most importantly, the $\gamma_{15}$ line that is identified with the symmetry of the porphyrin saddling deformation ($B_{2u}$) (*22*, *24*) gains considerable intensity at 699 $cm^{-1}$.

Because the spectrum at the lowest porphyrin concentration (0.1 molar ratio) somewhat resembles the RR spectrum of some ferric heme species and because ferric heme is known to be endogenously bound to the enzyme before $H_2$(ProtoP) is added, we examined the ferric heme content using the spectra in the Inset in Figure 4. The 0.1-ratio $H_2$(ProtoP)/ferrochelatase spectrum (Figure 4B, spectrum f) has the oxidation-state marker line $\nu_4$ at 1369 $cm^{-1}$. This line should be a mixture of a $\nu_4$ similar to the free $H_2$(ProtoP) in the detergent solution at 1368 $cm^{-1}$ (Figure 4B, spectrum e) and $\nu_4$ of the ferric heme that is endogenously bound to native ferrochelatase at 1373 $cm^{-1}$. The composition of this line was confirmed by the fact that hydrosulfite reduction of the 0.1-ratio sample gives a RR spectrum (Figure 4, spectrum g) that is a mixture of the shifted high-spin five-coordinate ferrous heme line and another spectral component from protein-bound $H_2$(ProtoP) that has a frequency that is very near the free $H_2$(ProtoP) in buffer (Figure 4B, spectrum e). Thus, endogenously bound ferric heme does make a contribution to the spectrum, at least for the oxidation-state marker line. Similar behavior is noted for $\nu_7$ in the low-frequency region (Inset of Figure 4A). Here, the difference between the bound and unbound $H_2$(ProtoP) frequencies is more evident.

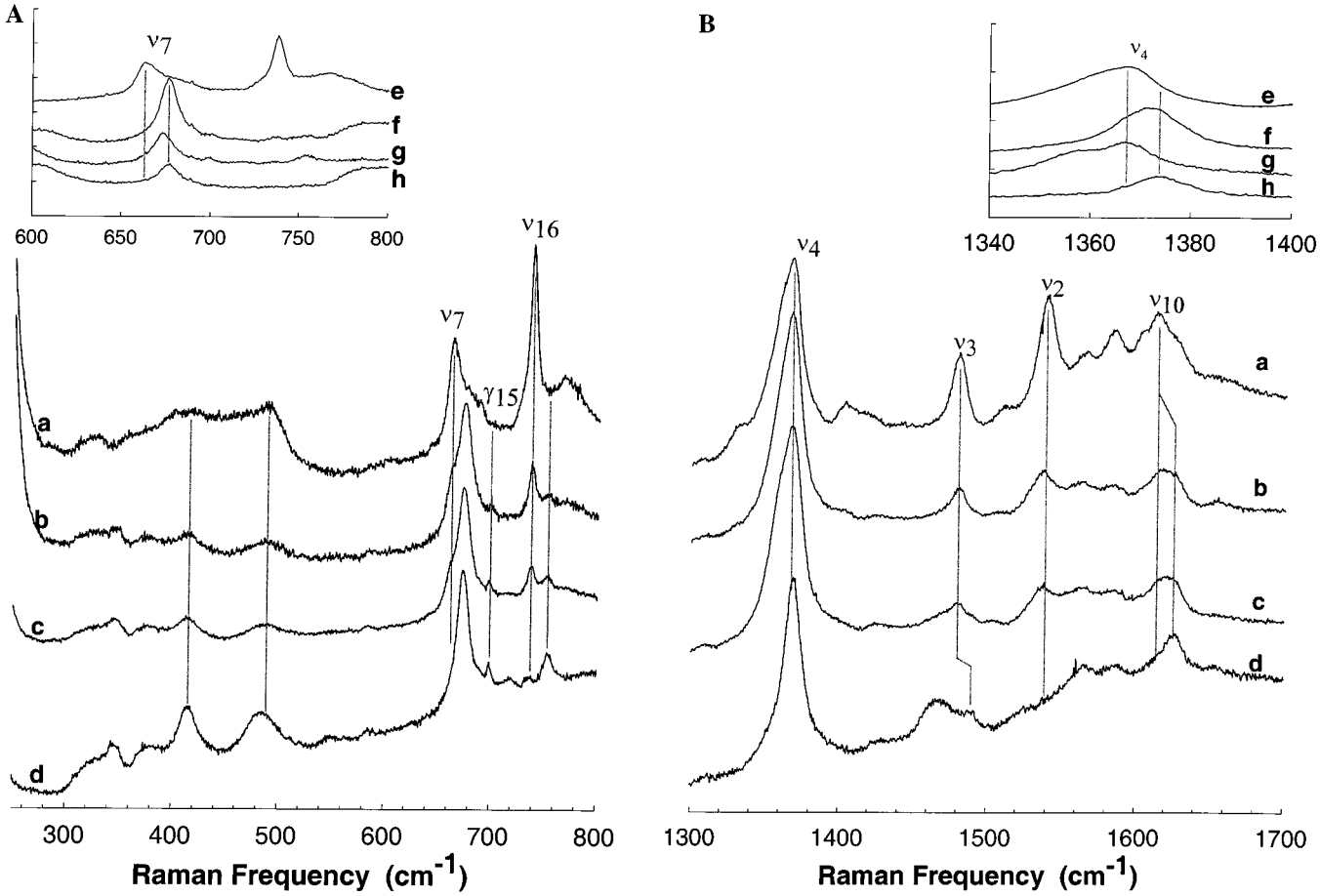


FIGURE 4: Low-frequency (A) and high-frequency (B) regions of the resonance Raman spectra of (a, e) $H_2$(ProtoP) in buffer H with detergent, and $H_2$(ProtoP) titration of native wild-type ferrochelatase at $H_2$(ProtoP)/protein ratios of (b) 1.0 (same concentration of $H_2$(ProtoP) as in spectrum a), (c) 0.5, and (d, f) 0.1. (Inset) RR spectra of (e) $H_2$(ProtoP) in buffered detergent solution, (f) $H_2$(ProtoP) added to native wild-type ferrochelatase at a $H_2$(ProtoP)/protein ratio of 0.1, (g) sodium hydrosulfite-reduction of this sample, and (h) native wild-type ferrochelatase.

## DISCUSSION

*Binding of Heme to Ferrochelatase.* As isolated, native ferrochelatase presents an endogenously bound porphyrin species that was not identified in our former work (*15*), but now it can be unambiguously attributed mostly to bound ferric heme. Some wild-type ferrochelatase preparations, including those of the previous work, exhibit this endogenously bound ferric heme in the high-spin state (*15*). In contrast, the protein preparations used in this work have the endogenously bound heme in the low-spin state based on the similarities in the RR spectra of various heme models. The reasons for the heme spin-state variation among different protein preparations have not been determined but might involve binding of trace metal ions or organic molecules at the active site. These species might come from different batches of reagents used in the preparation of the several protein purification buffers. Regardless of the spin state of this endogenously bound species, enzyme activity is not affected. It should be noted that the endogenously bound species can be estimated to be at most 2% of the protein concentration, based on the intensity of the RR spectrum of endogenously bound heme as compared to the spectrum of added ferric heme bound to ferrochelatase at a 0.1 ratio (Figures 1, spectum c, and 2, spectrum e). Added ferric heme also binds to ferrochelatase in the low-spin state based on the RR spectrum. Another factor in support of the endogenously bound ferric heme being a minor species is that the intense Soret absorption peak associated with this bound ferric heme cannot be distinguished from the iron−sulfur cluster absorption band in the spectrum of wild-type ferrochelatase. It should also be noted that an exogenous ligand, like imidazole, could be responsible for this spin state change. Imidazole is used during the purification procedure (see Materials and Methods). Although it is subsequently removed by a gel filtration step, variable amounts might stay bound to the active site of the enzyme. The possibility that exogenous imidazole can be an axial heme ligand and source of the low-spin state of the heme iron can be excluded because of the apparent almost complete binding (see the following discussion) in the low-spin state, even at one heme per protein, which rules out an imidazole impurity as the cause of the low-spin state.

Although the samples used in our studies are considered pure, metallic ions at less than stoichiometric ratios were detected in some of the protein preparations and could not be removed. These include nickel(II) and copper(II), which are common contaminants of buffers. These metals become visible in the RR spectra in the form of the corresponding metalloporphyrins when the contaminating metal ions are inserted into $H_2$(ProtoP) by the enzyme. The metal ion concentrations are typically a small fraction of the protein concentration. Extreme care is required in the sample

preparation of the enzyme with low concentrations of porphyrin. Nevertheless, the aforementioned observations about the ferrochelatase preparations (e.g., variable spin state of the endogenously bound ferric heme and contamination by metallic ions at below-stoichiometric ratios) are important only for the interpretation of some of the RR studies presented. However, they do not influence the enzymatic activity. In fact, all of the enzyme preparations were equally and highly active, as might be expected because contaminating free metal ions are removed from solution immediately at the beginning of the reaction by incorporation into free-base porphyrin. The concentrated enzyme preparations used for the RR study showed that almost no contaminating metal ions were incorporated into free-base porphyrin for these samples.

Upon reduction, the endogenously bound low-spin ferric heme converts to high-spin ferrous heme, thus confirming the identification of the endogenously bound species as heme. The same spin-state conversion was observed for exogenously added ferric heme that binds to the protein. Specifically, upon chemical reduction of a ferrochelatase sample at a ferric heme-to-protein ratio of 0.5, RR spectra revealed the presence of low-spin ferric heme before reduction and high-spin ferrous heme after reduction. UV−visible spectroscopy of ferrochelatase with added ferrous heme also revealed that the Fe(II)ProtoP binds to the protein as a high-spin form. It can be concluded that the endogenously bound ferric heme exhibits the same binding characteristics as exogenously added ferric heme, changing from high-spin to low-spin upon binding and then back to high-spin upon heme reduction.

In the high-frequency RR spectra obtained during titration of ferrochelatase with ferric heme (Figure 2B), the intensity of the 1489 $cm^{-1}$ line, characteristic of the unbound high-spin five-coordinate species, decreases steadily until undetectable at a ferric heme-to-protein ratio of 0.1. Concomitantly, the intensity of the 1503 $cm^{-1}$ line characteristic of the bound low-spin six-coordinate ferric heme increases. Assignment of relative concentrations based on the intensities of RR lines from these two species is not possible because the Raman lines have different intrinsic intensities due to different resonance enhancement factors. Thus, for the unbound form to not be seen in the RR spectra, the concentration must be reduced to a ferric heme-to-protein ratio of 0.1 (Figure 2B, spectrum e), but this cannot be taken to mean that the binding is not nearly stoichiometric. This could just mean that any unbound form that coexists in the sample may be contributing to the overall spectrum in a way that is not proportional to its actual concentration. UV−visible titration of ferrochelatase with ferric heme, performed as previously described (*15*), allows us to conclude that ferric heme is almost completely bound to the protein even at a 1.0 molar ratio, based on the equilibrium dissociation constant ($K_D$) which is in the micromolar range (data not shown). However, we cannot rule out the presence of another species, such as a weakly bound high-spin form whose spectrum is very similar to the unbound ferric heme in buffer.

*Binding of Nickel Protoporphyrin to Ferrochelatase.* Analysis of any porphyrin structural changes induced by binding of ferrochelatase to Ni(ProtoP) is facilitated by comparing the RR spectrum of Ni(ProtoP) to those of Ni(ProtoP)−ferrochelatase complexes. Because Ni(ProtoP) stays four-coordinated, the structural interpretation of the RR data is easier because axial coordination and spin state do not change upon binding. In our previous study (*15*), a downshift of RR lines was observed upon binding of Ni(ProtoP) to ferrochelatase at porphyrin/enzyme ratio of 1, and this downshift was a result of protein-induced porphyrin distortion. In the present study, we observe that porphyrin/enzyme ratios of less than 1, in the range between 0.1 and 0.5, result in slightly larger downshifts in the high-frequency RR lines $\nu_3$, $\nu_2$, and $\nu_{10}$, thereby suggesting slightly larger porphyrin distortions at substoichiometric porphyrin concentrations. The downshifts in these high-frequency structure-sensitive lines for all porphyrin concentrations studied indicate an increased out-of-plane distortion, probably ruffling because these RR lines are most sensitive to this particular type of macrocycle deformation (*15*). There is some additional evidence of a slightly increased distortion for the most strongly bound Ni(ProtoP) (i.e., porphyrin bound at the lowest concentrations); however, the lower RR frequencies could only result from less of a contribution to the spectrum from the unbound Ni(ProtoP).

Consistent with an interpretation of the high-frequency shift based on protein-induced distortion, the low-frequency structure-sensitive line $\nu_8$ also shifts and appears to split upon binding to ferrochelatase. The changes in $\nu_8$ can be interpreted in terms of important alterations in the macrocycle conformation or the conformations of the porphyrin substituents, as this line is sensitive to both influences. In addition, the out-of-plane mode $\gamma_6$ might also be present in the protein-bound forms near 354 $cm^{-1}$, slightly below 360 $cm^{-1}$ where it appears in Ni(OEP); $\gamma_6$ has been assigned to a porphyrin $A_{2u}$ symmetry (doming-type) mode (*22*, *24*). The change in this mode upon binding (Figure 3A) might indicate a contribution of a doming deformation to the protein-induced macrocycle distortion.

The apparent splitting of the $\nu_7$ Raman line (Figure 3A), which occurs in the presence of detergent and increases upon protein binding, is not observed in the RR spectra of nickel-reconstituted hemoglobin (Ni-Hb) (*26*−*28*). Because $\nu_7$ is not degenerate, one explanation for the $\nu_7$ splitting observed on the binding of Ni (ProtoP) to ferrochelatase is that there are two different vibrational modes, correlating to two different porphyrin environments. Alternatively, one of these modes might be $\gamma_{20}$, which is calculated to be at 713 $cm^{-1}$ for Ni(OEP). $\gamma_{20}$ might become more apparent as $\nu_7$ downshifts as a result of ferrochelatase chelation. $\gamma_{20}$ is a doubly degenerate out-of-plane $E_g$ mode that has been associated with porphyrin distortions such as those found in ferrous cytochrome *c*, for which the mode is assigned to a doublet found at 653/666 $cm^{-1}$ (*24*). On the basis of the available ferrochelatase crystal structures containing bound porphyrins (*11*), the porphyrin distortions predicted for ferrochelatase-bound Ni(ProtoP) include the wave ($E_g$) and dome ($A_{2u}$) deformations (see the following discussion).

Evidence that binding influences the conformations of the peripheral substituents as well as the macrocycle comes from changes in the propionate and vinyl modes of Ni(ProtoP). The two propionate modes in the low-frequency region of the RR spectra change intensities upon protein binding, suggestive of different porphyrin environments with a unique orientation for each of the vinyl groups. The same intensity ratio for these lines can be seen in apo-HbA reconstituted

with Ni(ProtoP). X-ray structure of Ni-Hb (PDB access codes 1NIH (*27*) and 1DKE (*28*)) reveals that the propionate groups are oriented in opposite directions, one above and one below the porphyrin plane. In some cases, one propionate is hydrogen-bonded to an arginine, whereas the other is not involved in any particular interaction. Thus, the intensity ratio for the propionate lines in the RR spectra of ferrochelatase could reflect similar interactions as those observed for Ni-Hb.

*Binding of Free-Base Protoporphyrin to Ferrochelatase.* For $H_2$(ProtoP) binding to ferrochelatase, the results obtained might also suggest significant nonplanar porphyrin distortion. Because all structure-sensitive lines in the high-frequency region strongly upshift upon binding to the protein, the bound free-base porphyrin is either subject to extensive distortion or to some other interaction with the protein. The RR spectra of $H_2$(ProtoP) bound to ferrochelatase are dominated by the unbound fraction, just as is the case for addition of ferric heme to ferrochelatase. Thus, it is only with the low concentrations of porphyrin, at which almost all of the porphyrin is bound, that we can clearly observe the RR spectrum of the bound form. Another interpretation is that there is a form which is bound to the enzyme, as indicated by the changes in the absorption spectrum, but which has a RR spectrum that is very much like the unbound porphyrin. In either case, only at a $H_2$(ProtoP)-to-protein ratio as small as 0.1 do we observe a nearly pure spectrum of the bound form, and it has a drastically altered porphyrin structure based on the frequency shifts. Apparently at higher concentration of porphyrin, a minor amount of the unbound species inordinately contributes to the overall RR spectrum, obscuring the spectrum of the strongly bound form.

*Increases* in frequency of the structure-sensitive marker lines, such as $\nu_3$ and $\nu_{10}$, are not typically associated with out-of-plane distortion of the porphyrin macrocycle, but the dependence of the marker line frequencies on distortion is based mostly on RR studies of metal derivatives and not on the free-base porphyrins. The macrocycle of metal porphyrin is much less flexible than for free-base porphyrins in molecular mechanics calculations. Molecular modeling shows that the increased macrocyclic flexibility of free-base porphyrins is a consequence of the lack of bonds across the central core of the porphyrin that are present in metal derivatives. The frequency dependence might also be different for a free-base porphyrin deformation than for the same deformation of a metalloporphyrin. In addition, the free-base porphyrin may interact with the protein through the protons and lone pairs of the nitrogens in the core, thus leading to increases in the structure-sensitive lines that are independent of the out-of-plane distortion.

Compelling evidence for distortion of the natural substrate of ferrochelatase comes from analysis of the low-frequency region of the RR spectra obtained from bound free-base porphyrin. Upon protein binding, the $\gamma_{15}$ mode appears at 699 $cm^{-1}$ as the $H_2$(ProtoP)/protein ratio decreases (Figure 4A). Its absence from the RR spectrum of native ferrochelatase indicates that it does not originate from the endogenously bound ferric heme. Furthermore, $\gamma_{15}$ does not change upon chemical reduction of the protein (see Inset in Figure 4A). Thus, it must come from the protein-bound $H_2$(ProtoP) species. $\gamma_{15}$ is a $B_{2u}$ symmetry (saddling-like) mode, and its appearance at 699 $cm^{-1}$ in the spectra of free-base protoporphyrin bound to ferrochelatase suggests that a saddling deformation occurs upon binding. This nonplanar porphyrin distortion occurs in murine ferrochelatase, even in the absence of the metal substrate.

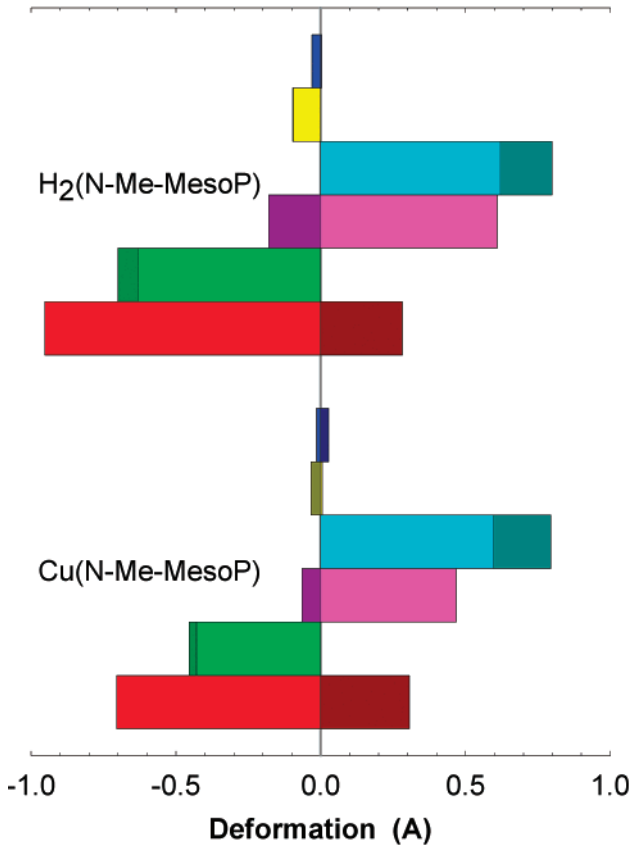


FIGURE 5: Normal-coordinate structural decomposition of the X-ray crystal structures (PDB codes 1CH1 and 1C9E) of porphyrins bound to *B. subtilis* ferrochelatase. Color coding: (red) saddling, (green) ruffling, (magenta) doming, (cyan) *x*-waving, (yellow) *y*-waving, (blue) propellering; light colors are for the lowest frequency mode of each symmetry type, and dark colors are for the next-to-lowest frequency mode of each symmetry type.

Figure 5 shows the normal-coordinate structural decomposition (NSD) of the porphyrins contained in the reported crystal structures of *B. subtilis* ferrochelatase (*11*). The major contributions to the distortion for Cu(N-Me-MesoP) and $H_2$(N-Me-MesoP) bound to ferrochelatase are saddling, followed by *x*-waving, ruffling, and doming. All of these, except for ruffling, are expected for isolated Cu- and $H_2$(N-Me-MesoP) because the pyrrole ring with the *N*-methyl group must be tilted out of porphyrin plane as a result of a combination of saddling, doming, and waving deformations. Thus, assuming that the structure of the mouse ferrochelatase active site induces similar distortions, it is not surprising that our RR data in this study provide support for the presence of all of these deformations for the ferrochelatase-bound porphyrins.

Several amino acid residues, which are conserved in the active site of ferrochelatase, are putative metal-ion binding ligands that could be responsible for the axial ligation observed for ferric heme and possible interaction with the core protons of free-base protoporphyrin. These could be oxygen/nitrogen-containing ligands as have been observed by Mössbauer spectroscopy of ferrous ion-reacted native

ferrochelatase (*29*). Further RR studies of site-directed variants will be instrumental in determining the identity of these ligands. Nevertheless, we can conclude that the high-frequency RR lines observed for ferric heme-bound ferrochelatase comes from a six-coordinate LS complex with at least one and maybe two strong-field axial ligands. The heme in the reduced ferrous heme−ferrochelatase complex exhibits RR lines that are consistent with a five-coordinate high-spin complex with histidine or tyrosine as the ligand (*30*, *31*). Because both histidine (e.g., H207 or H285) and tyrosine (e.g., Y109 or Y220) are near the active site of ferrochelatase, it is possible that the interaction of the free-base protons with one of these ligating groups accounts for the radically altered spectrum of bound free-base protoporphyrin and the coordination of heme.

## REFERENCES


1. Ferreira, G. C., Franco, R., Lloyd, S. G., Moura, I., Moura, J. J., and Huynh, B. H. (1995) *J. Bioenerg. Biomembr. 27*, 221−229.
2. Ferreira, G. C. (1994) *J. Biol. Chem. 269*, 4396−4400.
3. Dailey, H. A., Finnegan, M. G., and Johnson, M. K. (1994) *Biochemistry 33*, 403−407.
4. Al-Karadaghi, S., Hansson, M., Nikonov, S., Jönsson, B., and Hederstedt, L. (1997) *Structure 5*, 1501−1510.
5. Wu, C. K., Dailey, H. A., Rose, J. P., Burden, A., Sellers, V. M., and Wang, B. C. (2001) *Nat. Struct. Biol. 8*, 156−160.
6. Ferreira, G. C. (1995) *Biochem. Biophys. Res. Commun. 214*, 875−878.
7. Dailey, H. A., and Fleming, J. E. (1983) *J. Biol. Chem. 258*, 11453−11459.
8. Dailey, H. A., Jones, C. S., and Karr, S. W. (1989) *Biochim. Biophys. Acta 999*, 7−11.
9. Cochran, A. G., and Schultz, P. G. (1990) *Science 249*, 781−783.
10. Romesberg, F. E., Santarsiero, B. D., Spiller, B., Yin, J., Barnes, D., Schultz, P. G., and Stevens, R. C. (1998) *Biochemistry 37*, 14404−14409.
11. Lecerof, D., Fodje, M., Hansson, A., Hansson, M., and Al-Karadaghi, S. (2000) *J. Mol. Biol. 297*, 221−232.
12. Jentzen, W., Ma, J. G., and Shelnutt, J. A. (1998) *Biophys. J. 74*, 753−763.
13. Shelnutt, J. A. (2000) in *The Porphyrin Handbook* (Kadish, K. M., Smith, K. M., and Guilard, R., Eds.) pp 167−223, Academic Press, New York.
14. Shelnutt, J. A., Song, X. Z., Ma, J. G., Jia, S. L., Jentzen, W., and Medforth, C. J. (1998) *Chem. Soc. Rev. 27*, 31−41.
15. Franco, R., Ma, J. G., Lu, Y., Ferreira, G. C., and Shelnutt, J. A. (2000) *Biochemistry 39*, 2517−2529.
16. Blackwood, M. E., Jr., Rush, T. S., III, Romesberg, F., Schultz, P. G., and Spiro, T. G. (1998) *Biochemistry 37*, 779−782.
17. Franco, R., Pereira, A. S., Tavares, P., Mangravita, A., Barber, M. J., Moura, I., and Ferreira, G. C. (2001) *Biochem. J. 356*, 217−222.
18. Abbas, A., and Labbe-Bois, R. (1993) *J. Biol. Chem. 268*, 8541−8546.
19. Camadro, J. M., and Labbe, P. (1988) *J. Biol. Chem. 263*, 11675−11682.
20. Kuzelova, K., and Brault, D. (1994) *Biochemistry 33*, 9447−9459.
21. Falk, J. E. (1964) *Porphyrins and metalloporphyrins; their general, physical and coordination chemistry, and laboratory methods*, Elsevier Pub. Co., New York.
22. Hu, S., Smith, K. M., and Spiro, T. G. (1996) *J. Am. Chem. Soc. 118*, 12638−12646.
23. Jentzen, W., Unger, E., Song, X. Z., Jia, S. L., TurowskaTyrk, I., SchweitzerStenner, R., Dreybrodt, W., Scheidt, W. R., and Shelnutt, J. A. (1997) *J. Phys. Chem. A 101*, 5789−5798.
24. Hu, S., Morris, I. K., Singh, J. P., Smith, K. M., and Spiro, T. G. (1993) *J. Am. Chem. Soc. 115*, 12446−12458.
25. Li, X. Y., Czernuszewicz, R. S., Kincaid, J. R., and Spiro, T. G. (1989) *J. Am. Chem. Soc. 111*, 7012−7023.
26. Shelnutt, J. A., Alston, K., Ho, J. Y., Yu, N. T., Yamamoto, T., and Rifkind, J. M. (1986) *Biochemistry 25*, 620−627.
27. Luisi, B., Liddington, B., Fermi, G., and Shibayama, N. (1990) *J. Mol. Biol. 214*, 7−14.
28. Bruno, S., Bettati, S., Manfredini, M., Mozzarelli, A., Bolognesi, M., Deriu, D., Rosano, C., Tsuneshige, A., Yonetani, T., and Henry, E. R. (2000) *Protein Sci. 9*, 683−692.
29. Franco, R., Moura, J. J. G., Moura, I., Lloyd, S. G., Huynh, B. H., Forbes, W. S., and Ferreira, G. C. (1995) *J. Biol. Chem. 270*, 26352−26357.
30. Wang, J., Larsen, R. W., Moench, S. J., Satterlee, J. D., Rousseau, D. L., and Ondrias, M. R. (1996) *Biochemistry 35*, 453−463.
31. Liu, Y., Moenne-Loccoz, P., Hildebrand, D. P., Wilks, A., Loehr, T. M., Mauk, A. G., and de Montellano, P. R. O. (1999) *Biochemistry 38*, 3733−3743.


BI025569M